Lawrence Berkeley National Laboratory

Title

Hierarchically Ordered Nanopatterns for Spatial Control of Biomolecules

Permalink

https://escholarship.org/uc/item/8kf8m1c3

Authors

Tran, Helen
Ronaldson, Kacey
Bailey, Nevette A
et al.

Peer reviewed

Hierarchically Ordered Nanopatterns for Spatial Control of Biomolecules

Helen Tran,[†] Kacey Ronaldson,[‡] Nevette A. Bailey,[†] Nathaniel A. Lynd,[§] Kato L. Killops,[||] Gordana Vunjak-Novakovic,[‡] and Luis M. Campos*,[†]

[†]Department of Chemistry, Columbia University, New York, New York 10027, United States, [‡]Department of Biomedical Engineering, Columbia University, New York, New York 10027, United States, [§]McKetta Department of Chemical Engineering, The University of Texas at Austin, Austin, Texas 78712, United States, and [||]Edgewood Chemical Biological Center, Aberdeen Proving Ground, Maryland 21010, United States

ABSTRACT
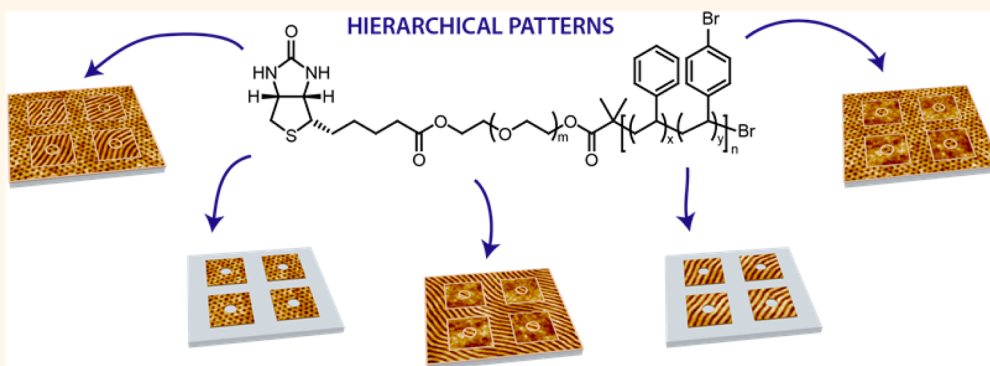
The development and study of a benchtop, high-throughput, and inexpensive fabrication strategy to obtain hierarchical patterns of biomolecules with sub-50 nm resolution is presented. A diblock copolymer of polystyrene-*b*-poly(ethylene oxide), PS-*b*-PEO, is synthesized with biotin capping the PEO block and 4-bromostyrene copolymerized within the polystyrene block at 5 wt %. These two handles allow thin films of the block copolymer to be postfunctionalized with biotinylated biomolecules of interest and to obtain micropatterns of nanoscale-ordered films *via* photolithography. The design of this single polymer further allows access to two distinct superficial nanopatterns (lines and dots), where the PEO cylinders are oriented parallel or perpendicular to the substrate. Moreover, we present a strategy to obtain hierarchical mixed morphologies: a thin-film coating of cylinders both parallel and perpendicular to the substrate can be obtained by tuning the solvent annealing and irradiation conditions.

KEYWORDS: block copolymer self-assembly · hierarchical patterns · dual protein patterning

Strategies to pattern biomolecules and small molecules have enabled the advancement of tissue engineering and genomics,[1−3] fabrication of biodevices,[4−6] development of microarray platforms for diagnostics and drug screening,[7,8] and investigation of fundamental cellular behavior.[9−13] Conventional lithography, contact-based stamping, block copolymer (BCP) self-assembly, and scanning probe lithography have been employed for generating arrays of diverse biomolecules ranging from short DNA sequences to fluorescent antibodies.[14−23] Each technique offers a combination of strengths and weaknesses in terms of biocompatibility, processing ease, resolution, speed, time and cost, and is amenable to specific applications.[24−28]

Current aims in patterning biomolecules with sub-50 nm resolution include immobilizing multiple types of proteins on a single substrate and constructing hierarchical architectures. The presentation of different proteins is an important step toward mimicking the complex biological constructs pervasive in nature, such as those involved in immune recognition, cell adhesion, and neuronal signaling.[29] There has been substantial progress in the fabrication of multicomponent proteins in the micrometer regime.[30−34] For sub-50 nm resolution, protocols often exhibit slow patterning speeds, complex fabrication, or poor control of protein positioning.[35] Analogous to multicomponent proteins, native-like hierarchical structures, such as primary to ternary
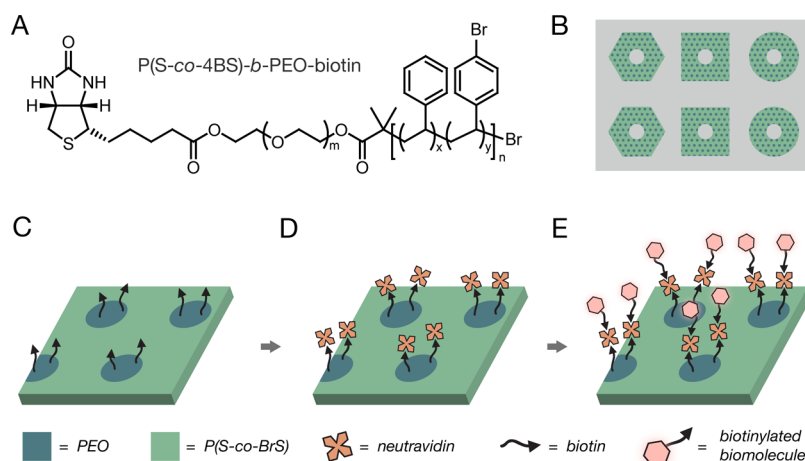
Figure 1. Hierarchical patterning. (A) Chemical structure of P(S-*co*-BrS)-*b*-PEO-biotin is shown. (B) Nanopatterning arises from BCP self-assembly and micropatterning is achieved by shadow-mask cross-linking. (C) Biotinylated PEO domains are postfunctionalized *via* the (D) biotin−neutravidin interaction, yielding (E) nanopatterns of biomolecules.

structure of proteins, have been generated and recent studies have demonstrated the importance of 2D hierarchical patterns of biomolecules in the form of modular surface shapes that span nano- to microscale structures.[36] Relatively few approaches are viable for hierarchical 2D patterning of biomolecules, including BCP micelle lithography coupled with photo- or electron-beam lithography,[37] scanning probe BCP lithography,[38] and other specialized microfabrication techniques,[36] which all exhibit similar aforementioned limitations.[36,39,40] Notably, techniques based on BCP micelle lithography are reliable and have led to insights of cell adhesion mechanisms; however, patterns are limited to dot arrays of inorganic nanoparticles.[41] A robust, facile, and high-throughput technique for hierarchical patterning of multiple types of biomolecules in multiple morphologies with sub-50 nm resolution is needed to drive the use of functionalized substrates for biological studies and screening technologies.

Here, we present a bottom-up/top-down method for achieving hierarchical patterns of biomolecules through the self-assembly of a functional BCP coupled with photolithography (Figure 1). Biomolecule patterning *via* BCP self-assembly is attractive because of its ease, high-throughput nature, and ability to access nanoscale features.[42−48] Among the various types of BCPs, polystyrene-*b*-poly(ethylene oxide) (PS-*b*-PEO) was chosen as the parent system due to its well established self-assembly behavior upon solvent vapor annealing.[49,50] Two functional handles were incorporated to the parent BCP: biotin for modular postfunctionalization and 4-bromostyrene (BrS) for cross-linking. The numerous advantages of using biotin stem from its ubiquitous, high-affinity, specific interaction with neutravidin as a modular linker to introduce biotinylated biomolecules of interest. Thus, myriad biofunctional constructs can be accessed *via* a single polymer platform. Additionally, shadow-mask irradiation

TABLE 1. Family of BCPs Based on PS-*b*-PEO

polymer	total $M_n{}^a$	wt % PEO^b	dispersity^a
PS-*b*-PEO	31,000	24	1.04
PS-*b*-PEO-biotin	31,000	24	1.04
P(S-*co*-BrS)-*b*-PEO-biotin	37,000	26	1.21

^{a} By SEC. ^{b} By NMR.

of cross-linkable thin films containing BrS with 254 nm light yields micropatterns after removal of uncrosslinked regions.[51] P(S-*co*-BrS)-*b*-PEO-biotin (Figure 1) offers a versatile platform for hierarchical patterning of biomolecules with sub-50 nm resolution and three distinct nanoscale morphologies.

RESULTS AND DISCUSSION

To carry out the appropriate controls to biofunctionalize hierarchical patterns, a family of PS-*b*-PEO derivatives was synthesized, where BCPs exhibit relative weight fractions characteristic for cylindrical morphologies (Table 1).[52] The minority block, PEO, is the cylindrical domain embedded in the matrix of the majority block, PS. In this family of BCPs, PS-*b*-PEO serves as the nonfunctional control, PS-*b*-PEO-biotin is biofunctional but not cross-linkable, and P(S-*co*-BrS)-*b*-PEO-biotin represents the system for hierarchical patterning of biomolecules. While the relative volume ratios and total molecular weight of each block direct the nanoscale morphology and size of the microdomains formed upon self-assembly, the orientation of these microdomains with respect to the substrate is directed by the film thickness and solvent vapor annealing conditions. Atomic force microscopy (AFM) images of as cast thin films of all the polymers were featureless. Upon solvent annealing, AFM images of PS-*b*-PEO (Figure 2A, 2D), PS-*b*-PEO-biotin (Figure 2B, 2E), and P(S-*co*-BrS)-*b*-PEO-biotin (Figure 2C, 2F) show
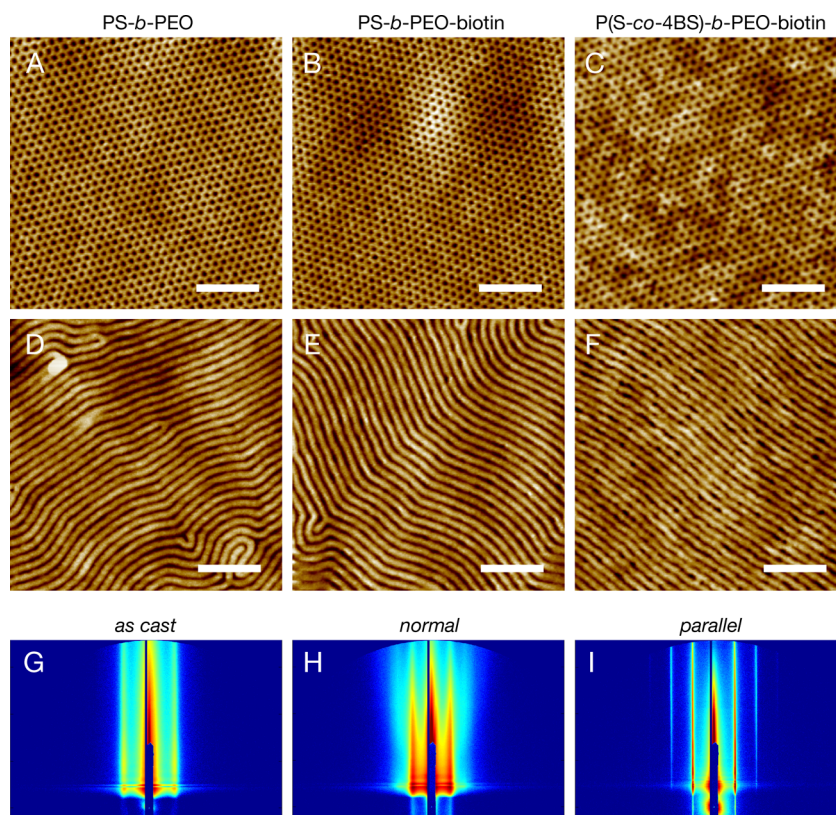
Figure 2. Thin film morphologies. (A−F) Atomic force microscopy images of solvent vapor annealed thin films of (A and D) PS-*b*-PEO, (B and E) PS-*b*-PEO-biotin, and (C and F) P(S-*co*-BrS)-*b*-PEO-biotin. Morphology is confirmed with grazing-incidence small-angle X-ray scattering for (G) as cast, (H) normal, and (I) parallel structures. Scale bar is (A−F) 200 nm.

PEO cylinders oriented normal or parallel to the substrate, superficially displaying dots or lines, respectively. Each BCP affords access to two well-defined, nanometer-sized morphologies with minor adjustments to the processing conditions. Briefly, exposure to toluene/water or benzene vapors yielded PEO cylinders oriented normal or parallel to the substrate, respectively. Solvent vapor annealing was a suitable approach for thin-film self-assembly because of its ease, speed, and lack of substrate dependence. These nanoscale patterns were reliably and reproducibly obtained on glass slides, gold-coated glass slides, and silicon wafers.

Grazing-incident small-angle X-ray scattering (GISAXS) patterns of self-assembled thin films of PS-*b*-PEO-biotin confirmed the nanoscale cylindrical morphology and orientation relative to the substrate that was observed by AFM (Figure 2G−I). The as cast morphology displays a single peak at $q_y = 0.471$ nm^{-1} ($d = 13.3$ nm) and shifts to lower q_y upon solvent vapor annealing (Supporting Information Figure S1). For cylinders normal to the substrate, $q_y = 0.199, 0.345, 0.407,$ and 0.530 nm^{-1} ($d = 31.6, 18.2, 15.4,$ and 11.8 nm, respectively) were observed, exhibiting a characteristic $1, \sqrt{3}, \sqrt{4},$ and $\sqrt{7}$ pattern for cylinders packed in a hexagonal array. For cylinders parallel to the substrate, $q_y = 0.226, 0.449,$ and 0.675 nm^{-1} ($d = 27.8, 14.0,$ and 9.3 nm) were observed,

as expected for an effective in-plane line surface pattern arising from laying-down cylinders. The presence of higher order peaks is indicative of high ordering in the thin films.

P(S-*co*-BrS)-*b*-PEO-biotin contains BrS copolymerized with styrene at 5 wt % to minimize its effect on the self-assembly behavior while maintaining robust cross-linking. The photoactivated cross-linking of S-*co*-BrS avoids the need for photoresists, thus rendering this system more suitable for high-throughput biocompatible applications. To fabricate hierarchical patterns, the self-assembled BCP thin films were aligned with a commercially available lithographic quartz mask containing chromium micropatterns and subsequently cross-linked with 254 nm in a nitrogen atmosphere (Figure 3A and Supporting Information Figure S2). Similar to a negative photoresist, the chromium micropatterns effectively block exposure to irradiation, leaving such regions uncross-linked and soluble in dichloromethane to be rinsed away. A bright field image displays micropatterns of P(S-*co*-BrS)-*b*-PEO-biotin on 280 nm silicon dioxide (Figure 3F), whereas the nanopatterns were observed by AFM (Supporting Information Figure S3B). Notably, the fidelity of the nanopatterns was slightly lost after the dichloromethane washes and required a second round of solvent annealing, but for a reduced amount of time, to
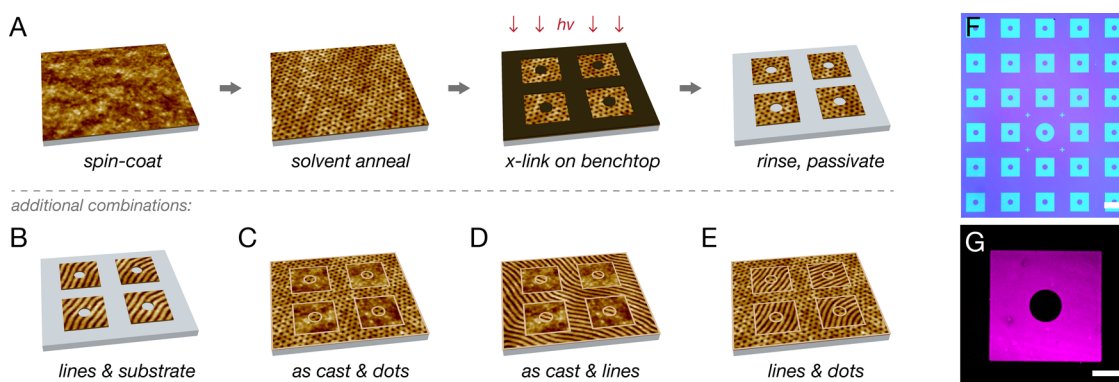
Figure 3. Protocol for fabrication of hierarchical patterns. (A) Illustration of general scheme for micropatterning microphase-segregated thin films of BCPs containing 4-bromostyrene to fabricate hierarchical patterns. **(B and C)** Illustrations of additional combinations of hierarchical morphologies accessible upon permutation of processing steps. **(F)** A bright field image showing an array of hierarchical patterns on 280 nm silicon dioxide. **(G)** Fluorescent hierarchical pattern upon incubation with streptavidin conjugated with Alexa-Fluor 647. **(A−F)** For clarity, illustrations are not to scale in order to simultaneously show nanopatterns and micropatterns. Scale bar is (F) 500 μm and (G) 150 μm.

regain the well-ordered microphase segregation (Supporting Information Figure S3). When a similar process was applied to PS-*b*-PEO and PS-*b*-PEO-biotin, BCPs that do not contain BrS, the entire film was soluble when rinsed with dichloromethane. This demonstrates the importance of BrS as a cross-linkable unit to generate the hierarchical patterns.

Control of domain orientation in specific regions of a substrate poses as a potentially valuable technique to simultaneously investigate multiple nanoscale patterns of biomolecules within micron-sized shapes. Previously reported techniques for dual presentation of nanoscale morphologies on a single substrate typically require substrate modification or specialized equipment.[53−56] For P(S-*co*-BrS)-*b*-PEO-biotin, dual presentation of morphologies is accessible by omitting the dichloromethane washes and permuting the solvent vapor annealing and cross-linking processes (Supporting Information Figure S4). Combinations of dots, lines, and featureless coatings are accessible (Figure 3A−E and Supporting Information Figure S4). For instance, a single substrate can be designed to display both line and dot morphologies (Figure 3E). Thin films of P(S-*co*-BrS)-*b*-PEO-biotin were spin-coated and solvent vapor annealed to yield lines. Micron-sized patterns were exposed to UV irradiation, effectively locking in the nanoscale morphology of the cross-linked regions. Then, the substrates were exposed to benzene vapor to switch the uncross-linked regions from lines to dots. The boundary region of these mixed morphology nanopatterns was observed by AFM, and clearly shows the transition between cylinders normal and parallel relative to the surface (Supporting Information Figure S4D).

By introducing biotin through end-functionalization of the PEO block, self-assembled thin films of PS-*b*-PEO-biotin contain biotin localized in the PEO domains and serve as a modular template to pattern biomolecules of interest with single protein precision (Figure 1).

Postfunctionalization with neutravidin−biotin motifs is an attractive approach because biomolecules are incorporated under mild conditions, biotinylated compounds are commercially available or easily prepared, and self-assembly conditions do not need to be optimized for each biomolecule, unlike the self-assembly of covalently modified polymers (Figure 1C-E).[46,57] With this modular approach, we can achieve a library of biofunctional arrays quickly using a single polymer platform. Biotinylated PS-*b*-PEO has been previously synthesized; however, annealing conditions yielded pseudo-hexagonally packed PEO cylinders, as opposed to the highly ordered films we describe here, and those studies were limited to the immobilization of streptavidin.[58]

By incubating hierarchical patterns of P(S-*co*-BrS)-*b*-PEO-biotin with streptavidin conjugated with Alexa Fluor 647, we visualized the fluorescent micropatterns by confocal microscopy and total internal reflection fluorescence (TIRF) microscopy (Figure 3G and Supporting Information Figure S5). The nanopatterns cannot be exclusively resolved with TIRF and our initial attempts to image with stochastic optical reconstruction microscopy for subdiffraction-limited resolution were unsuccessful. *Via* TIRF, fluorescence was not observed for PS-*b*-PEO which lacks the biotin handle essential to immobilize the fluorescent dye (Supporting Information Figure S5A). Alternatively, PS-*b*-PEO-biotin displayed high fluorescence (Supporting Information Figure S5B). For the hierarchical patterns fabricated on glass, the background fluorescence of the glass substrate was similar to the fluorescence observed for thin films of PS-*b*-PEO and the region of P(S-*co*-BrS)-*b*-PEO-biotin fluoresced similarly to PS-*b*-PEO-biotin. Fluorescence from streptavidin conjugated with Alexa Fluor 647 was exclusively observed within the biotinylated regions.

The ability to simultaneously pattern two proteins without synthetic changes to the BCP nor biomolecule of interest can be challenging.[43] Fabrication of
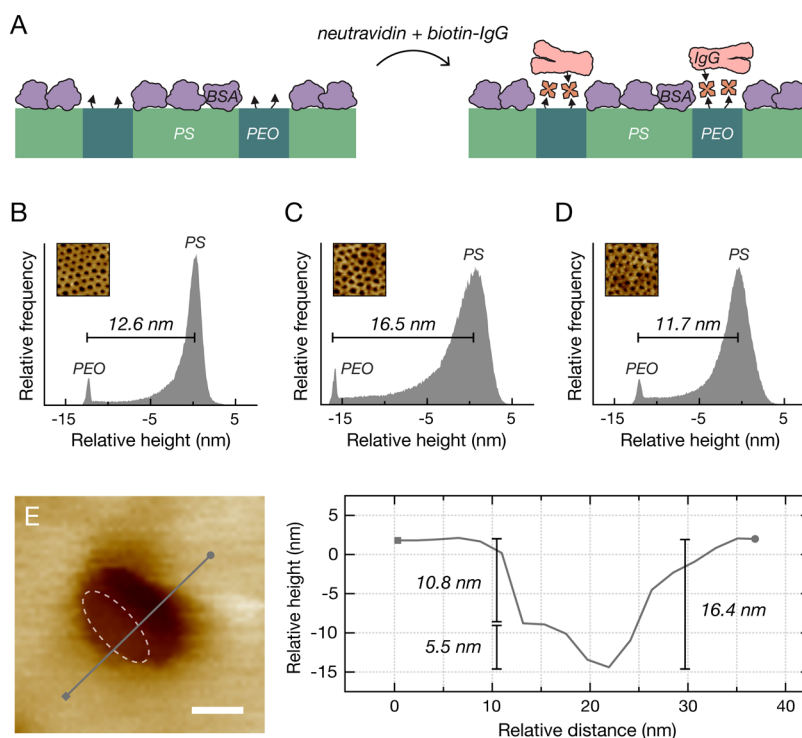
Figure 4. Dual protein functionalization. (A) Schematic for dual functionalization *via* hydrophobic and site-specific interactions. Frequency histograms of height differences on thin films of PS-*b*-PEO-biotin (B) before and (C) after incubation with BSA and (D) subsequently neutravidin/biotinylated-IgG. (E) Magnified view of PEO cylinder after BSA passivation and incubation with neutravidin/biotinylated-IgG and corresponding line cut. Scale bar is 7 nm.

multicomponent biomolecule arrays have been previously demonstrated and typically relies on lithography for patterning or activation,[30,31] sequential contact-based stamping,[32,33] scanning probe lithography with multiple inks,[35] complementary click reactions,[31] and selective adsorption on block copolymer thin films.[59] Here, we demonstrate that the combination of non-specific and site-specific interactions can be utilized to pattern two different proteins (Figure 4A). A frequency histogram of relative heights in a 1 μm^2 region of a flattened topographical AFM image of a self-assembled PS-*b*-PEO-biotin thin film displays a superficial difference of 12.6 nm between PS and PEO after swelling in phosphate-buffered saline (PBS) for 18 h (Figure 4B). The lower peak corresponds to PEO and the higher peak corresponds to PS. Incubation of the PS-*b*-PEO-biotin thin film in a solution of bovine serum albumin (BSA) resulted in selective physisorption of BSA on the PS domains (Figure 4A,C). BSA did not adhere on the PEO domains given that PEO prevents nonspecific adhesion. With PS selectively covered with BSA, we observed an increase in the difference of relative heights of 16.5 nm, where 3.9 nm approximately correlates to the height of a BSA protein (Figure 4C). Further incubation with neutravidin followed by biotin— IgG resulted in high bioaffinity interactions with the biotin on the PEO domains (Figure 4A). Compared to thin films of PS-*b*-PEO-biotin where PS regions were passivated by BSA (Figure 4C), we expected a decrease

of relative heights since neutravidin and biotin-IgG are localized in the PEO domains. We observed an 11.7 nm relative height difference with 4.8 nm decrease. A magnified view of a single PEO domain shows a single oblong shape, which may be attributed to a single IgG with its long axis oriented parallel to the substrate (Figure 4E). The corresponding line scan shows a height of 5.5 nm and width of 7 nm, consistent with previously reported AFM images of IgG.[43] In this case, IgG binding on the PEO domains was driven by the biotin-neutravidin active site on the BCP coating. These experiments highlight the ability to localize two important biomolecules within the same substrate by using nonspecific and site-specific interactions.[14,24,37]

Given the broad implications of these coatings for various applications, we sought to investigate the biocompatibility of the hierarchical coatings for cultivation with human mesenchymal stem cells (hMSCs). Hierarchical patterns with nanoscale dot patterns were prepared and subsequently biofunctionalized with neutravidin then biotin-RGD.[60] Rather than silicon or glass, gold-coated glass substrates were utilized to allow facile background passivation with oligoethylene glycol, which prevents cell adhesion that is typically observed on glass (Supporting Information Figures S6 and S7). hMSCs showed confinement within the hierarchical patterns (Figure 5A,B, and Supporting Information). Focal adhesions were visualized using vinculin staining, and we found them to be prominently distributed
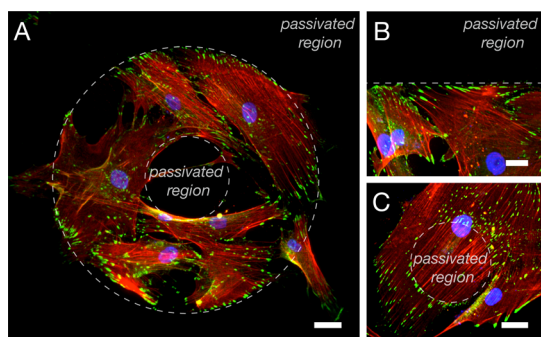
Figure 5. Patterning of human cells. (A–C) Human mesenchymal stem cells grown on hierarchical patterns fabricated with P(S-*co*-BrS)-*b*-PEO-biotin on gold-coated glass substrates passivated with oligoethylene glycol and stained for actin (red), vinculin (green), and nuclei (blue). Scale bar is 50 μm.

throughout the cell as well as at the edges. Previous studies of micrometer-sized shapes showed focal adhesions mostly localized at the periphery. We observed that a cell occasionally spreads into the passivated regions but lacks the formation of strong focal adhesions (Figure 5C). When cells are seeded onto passivated oligoethylene glycol surfaces, spreading is prevented and the cell assumes a round morphology (Supporting Information Figure S8). These observations have triggered ongoing studies to investigate in detail cell–substrate interactions using various hierarchical patterns. These hierarchical patterns enable, for the first time, the presentation of biomolecules with

hierarchical order, originating from a single BCP, using simple and robust benchtop processing.

CONCLUSION

Through bottom-up self-assembly and top-down photolithography, we demonstrate generation of hierarchical patterns of biomolecules with sub-50 nm resolution using P(S-*co*-BrS)-*b*-PEO-biotin. The three key morphologies are composed of as-cast (featureless), cylinders normal to the surface (dots), and cylinders parallel to the surface (lines) to the substrate, and can be produced on silicon, glass, or gold. In these thin films, BrS serves as a robust, *in situ* cross-linkable unit without compromising the self-assembly behavior of the BCP. By altering the solvent vapor annealing, cross-linking, and rinsing processing steps, various hierarchical combinations of the three nanoscale morphologies can be achieved. Further functionalization of the biotinylated PEO domains yields hierarchical presentation of biomolecules. These patterns can enable in-depth studies of cell adhesion, motility, and differentiation, among other mechanisms, using hierarchical patterns of biomolecules. Here, we demonstrated a viable strategy for the development of sophisticated 2D patterns from a modular BCP. In future studies, we envision that this technology will allow us to pattern various biologically active molecules at well-defined positions, presented in various hierarchical mixed morphologies, to dissect their activity, influence of hierarchical shapes and interactions with living cells.

METHODS

Block Copolymer Self-Assembly. Thin films were prepared by spin coating filtered (0.45 μm) 1 wt % (10 mg/mL) solutions of polymer at varying speeds on glass or silicon substrates. Solutions were stirred for ~12 h. Silicon, Au/Ti/glass and glass substrates were cleaned by sonication in DI water (30 min), acetone (2 × 15 min), 2-propanol (2 × 15 min) and dried with a nitrogen stream. For self-assembly, all films were annealed for 1–12 h and subsequently quenched with in a high humidity atmosphere for 2 min (RH 90–95%). Chips were placed on a glass tray under an inverted crystallization dish (o.d. × H 150 mm × 75 mm) with 2 × 10 mL beakers of solvent. For cylinders normal to the substrate, thin films were spin coated from dry toluene or benzene at 3000 rpm and annealed with a toluene/water vapor (2 × 10 mL toluene and 1 × 1 mL water) for 2–12 h. Long-range order improved with longer annealing times, but extended annealing times may lead to dewetting. For cylinders parallel to the substrates, thin films were spin coated from dry benzene at 3000 rpm and annealed with benzene vapor (2 × 10 mL benzene) for 1–6 h. Self-assembly was confirmed *via* atomic force microscopy in at least three distinct locations per substrate to confirm uniformity.

Micropatterning and Passivation. In a nitrogen atmosphere, self-assembled thin films were subjected to 254 nm irradiation for 25 min. UVP Black-Ray UV Bench Lamp XX-15S 254 nm was used for cross-linking. Extended irradiation times may lead to thin film etching. A quartz mask with chromium micropatterns was used. Chips were put in contact with the chromium mask *via* a homemade setup (Supporting Information Figure S2B) that is similar to a traditional mask aligner. To remove uncross-linked material to achieve micropatterns, samples were submerged in

dichloromethane (0.45 μm filtered) and the solvent was exchanged for 20 min. Then, samples were dried with a nitrogen stream and subjected to a second round of solvent annealing. For passivation of the 10 nm thick gold on glass, substrates were immersed in a 2 mM solution of triethylene glycol mono-11-mercaptoundecyl ether (EG3) in 200 proof ethanol for 24 h. Attention was given to avoid evaporation of the solution by sealing the container with parafilm. Subsequently, substrates were rinsed with 200 proof ethanol (5 × 5 mL, 1 min.), soaked for 2 h, then dried with a nitrogen stream.

Biofunctionalization. Thin films were swelled in 1× phosphate-buffered saline (PBS) without calcium/magnesium (pH = 7.4) for 18 h prior to biofunctionalization. All biofunctionalizations were carried out in 12 well plates at room temperature. For neutravidin conjugation, substrates were transferred to a well containing 2 mL of 10 μg/mL neutravidin in PBS for 30 min, then washed with PBS (4 mL, 5 × 5 min). For biotin–CRGDS conjugation, substrates previously functionalized with neutravidin were transferred to a well containing 2 mL of 10 μg/mL biotin–CRGDS in PBS for 30 min, then washed with PBS (4 mL, 5 × 5 min.). For biotin–DNA–Cy3 conjugation, substrates previously functionalized with neutravidin were transferred to a well containing 2 mL of 1 pM biotin–DNA–Cy3 and shaken for 10 min in the dark, then washed with PBS (6 mL, 3 × 15 min). For streptavidin–Alexa Fluor 647 conjugation, substrates were transferred to a well containing 2 mL of 10 μg/mL streptavidin–Alexa Fluor 647 for 10 min in the dark, then washed with PBS (6 mL, 3 × 15 min). For the dual protein studies, samples were first incubated in 100 μg/mL of BSA for 30 min then washed with PBS (4 mL, 2 × 1 min) for full coverage of the PS matrix with BSA. Then, substrates were functionalized with neutravidin

(described above) and followed with incubation with 2 mL of 10 μg/mL biotin$-$IgG for 30 min and a PBS wash (4 mL, 2 $\times$ 1 min.).

Characterization. All Nuclear Magnetic Resonance (NMR) spectra were recorded on a Bruker instrument at 400 MHz at room temperature. Chemical shifts for ^{1}H NMR spectra are reported in parts per million downfield from Me$_4$Si and were referenced to residual protonated solvent (CDCl$_3$: δ 7.26). The M_n and dispersity of the polymers were obtained with size exclusion chromatography (SEC) with THF as the elutant and calibrated to linear PS standards. ScanAsyst and PeakForce tapping mode scanning force microscopy images were carried out using ScanAsyst-Air cantilevers (nominal spring constant = 0.4 N m^{-1} and resonance frequency = 70 kHz). An in-house TIRF system was used. Fluorescence images were collected on a Zeiss LSM 700 confocal microscope and were acquired using Zen 2010 software (Carl Zeiss, Inc.). GISAXS data was collected on the 8-IDE beamline at the Advanced Photon Source.

Cell Culture and Labeling. Annealed and passivated hierarchical patterns of P(S-co-BrS)-b-PEO-biotin were swelled overnight in 1$\times$ phosphate-buffered saline (PBS). All following steps were performed in a cell culture hood. For sterilization purposes, substrates were placed in a 6-well plate and incubated in antifungal-antibacterial solution for 30 min, then rinsed with 5 mL of 1$\times$ PBS (3 $\times$ 5 min). Human mesenchymal stem cells were maintained in tissue flasks in Dulbecco's modified eagle media (DMEM) with 10% fetal bovine serum (FBS), 1% penicillin$-$streptomycin (P/S) at 37 °C, and 5% CO$_2$. At 70% confluency, cells were trypsinized, resuspended with media, and seeded on the substrates at 1 $\times$ 10^6 cells/well. After 1 h, substrates were rinsed with media (3 $\times$ 5 mL) and maintained at 37 °C and 5% CO$_2$ for 18 h. At this point, all steps were performed outside of a cell culture hood. Cells were fixed with 4% paraformaldehyde for 15 min and rinsed with 1$\times$ PBS (3 $\times$ 5 mL). Then, cells were permeabilized with 2 mL Triton-X-100 in Tris-buffered saline for 5 min and rinsed with PBS (3 $\times$ 5 mL). Cells were incubated in antivinculin primary antibody solution at a 1:100 dilution (1$\times$ PBS, 0.1% BSA, 10% goat serum) for 24 h and rinsed with 1$\times$ PBS and 1 M NaCl (3 $\times$ 5 mL). Then, cells were incubated with the fluorescently labeled secondary antibody at 1:200 dilution (1$\times$ PBS, 0.1% BSA, 10% goat serum) for 1 h. Actin was stained with ActinRed 555 ReadyProbes for 30 min and rinsed with 1$\times$ PBS and 1 M NaCl. Lastly, nuclei was stained with NucBlue Fixed Cell ReadyProbes Reagent for 10 min and rinsed with 1$\times$ PBS and 1 M NaCl.

REFERENCES AND NOTES

1. Dvir, T.; Timko, B. P.; Kohane, D. S.; Langer, R. Nanotechnological Strategies for Engineering Complex Tissues. *Nat. Nanotechnol.* **2011**, *6*, 13–22.
2. Lutolf, M. P.; Hubbell, J. A. Synthetic Biomaterials as Instructive Extracellular Microenvironments for Morphogenesis in Tissue Engineering. *Nat. Biotechnol.* **2005**, *23*, 47–55.
3. Place, E. S.; Evans, N. D.; Stevens, M. M. Complexity in Biomaterials for Tissue Engineering. *Nat. Mater.* **2009**, *8*, 457–470.
4. Timko, B. P.; Cohen-Karni, T.; Qing, Q.; Tian, B.; Lieber, C. M. Design and Implementation of Functional Nanoelectronic Interfaces With Biomolecules, Cells, and Tissue Using Nanowire Device Arrays. *IEEE Trans. Nanotechnol.* **2010**, *9*, 269–280.
5. Reches, M.; Gazit, E. Casting Metal Nanowires Within Discrete Self-Assembled Peptide Nanotubes. *Science* **2003**, *300*, 625–627.
6. Zhang, S. Fabrication of Novel Biomaterials through Molecular Self-Assembly. *Nat. Biotechnol.* **2003**, *21*, 1171–1178.
7. Romanov, V.; Davidoff, S. N.; Miles, A. R.; Grainger, D. W.; Gale, B. K.; Brooks, B. D. A Critical Comparison of Protein Microarray Fabrication Technologies. *Analyst* **2014**, *139*, 1303–1326.
8. Hsiao, S. C.; Liu, H.; Holstlaw, T. A.; Liu, C.; Francis, C. Y.; Francis, M. B. Real Time Assays for Quantifying Cytotoxicity with Single Cell Resolution. *PLoS One* **2013**, *8*, e66739.
9. Orner, B. P.; Derda, R.; Lewis, R. L.; Thomson, J. A.; Kiessling, L. L. Arrays for the Combinatorial Exploration of Cell Adhesion. *J. Am. Chem. Soc.* **2004**, *126*, 10808–10809.
10. Bettinger, C. J.; Langer, R.; Borenstein, J. T. Engineering Substrate Topography at the Micro- and Nanoscale to Control Cell Function. *Angew. Chem., Int. Ed.* **2009**, *48*, 5406–5415.
11. Wan, L. Q.; Ronaldson, K.; Park, M.; Taylor, G.; Zhang, Y.; Gimble, J. M.; Vunjak-Novakovic, G. Micropatterned Mammalian Cells Exhibit Phenotype-Specific Left-Right Asymmetry. *Proc. Natl. Acad. Sci. U.S.A.* **2011**, *108*, 12295–12300.
12. McMurray, R. J.; Gadegaard, N.; Tsimbouri, P. M.; Burgess, K. V.; McNamara, L. E.; Tare, R.; Murawski, K.; Kingham, E.; Oreffo, R. O. C.; Dalby, M. J. Nanoscale Surfaces for the Long-Term Maintenance of Mesenchymal Stem Cell Phenotype and Multipotency. *Nat. Mater.* **2011**, *10*, 637–644.
13. Chen, C. S.; Mrksich, M.; Huang, S.; Whitesides, G. M.; Ingber, D. E. Geometric Control of Cell Life and Death. *Science* **1997**, *276*, 1425–1428.
14. Kolodziej, C. M.; Maynard, H. D. Electron-Beam Lithography for Patterning Biomolecules at the Micron and Nanometer Scale. *Chem. Mater.* **2012**, *24*, 774–780.
15. Akbulut, O.; Yu, A. A.; Stellacci, F. Fabrication of Biomolecular Devices *via* Supramolecular Contact-Based Approaches. *Chem. Soc. Rev.* **2009**, *39*, 30–37.
16. Liu, W.; Li, Y.; Yang, B. Fabrication and Applications of the Protein Patterns. *Sci. China Chem.* **2013**, *56*, 1087–1100.
17. Malmström, J.; Travas-Sejdic, J. Block Copolymers for Protein Ordering. *J. Appl. Polym. Sci.* **2014**, *131*, 40360.
18. Chai, J.; Wong, L. S.; Giam, L.; Mirkin, C. A. Single-Molecule Protein Arrays Enabled by Scanning Probe Block Copolymer Lithography. *Proc. Natl. Acad. Sci. U.S.A.* **2011**, *108*, 19521–19525.
19. Wu, C.-C.; Reinhoudt, D. N.; Otto, C.; Subramaniam, V.; Velders, A. H. Strategies for Patterning Biomolecules with Dip-Pen Nanolithography. *Small* **2011**, *7*, 989–1002.
20. Kilian, K. A.; Bugarija, B.; Lahn, B. T.; Mrksich, M. Geometric Cues for Directing the Differentiation of Mesenchymal Stem Cells. *Proc. Natl. Acad. Sci. U.S.A.* **2010**, *107*, 4872–4877.
21. Théry, M. Micropatterning as a Tool To Decipher Cell Morphogenesis and Functions. *J. Cell Sci.* **2010**, *123*, 4201–4213.
22. Huang, J.; Gräter, S. V.; Corbellini, F.; Rinck, S.; Bock, E.; Kemkemer, R.; Kessler, H.; Ding, J.; Spatz, J. P. Impact of Order and Disorder in RGD Nanopatterns on Cell Adhesion. *Nano Lett.* **2009**, *9*, 1111–1116.
23. Wang, X.; Yan, C.; Ye, K.; He, Y.; Li, Z.; Ding, J. Effect of RGD Nanospacing on Differentiation of Stem Cells. *Biomaterials* **2013**, *34*, 2865–2874.
24. Tran, H.; Killops, K. L.; Campos, L. M. Advancements and Challenges of Patterning Biomolecules with Sub-50 nm Features. *Soft Matter* **2013**, *9*, 6578–6586.

25. Ekerdt, B. L.; Segalman, R. A.; Schaffer, D. V. Spatial Organization of Cell-Adhesive Ligands for Advanced Cell Culture. *Biotechnol. J.* **2013**, *8*, 1411–1423.

26. Christman, K. L.; Enriquez-Rios, V. D.; Maynard, H. D. Nanopatterning Proteins and Peptides. *Soft Matter* **2006**, *2*, 928–939.

27. Huang, J.; Ding, J. Nanostructured Interfaces with RGD Arrays To Control Cell−Matrix Interaction. *Soft Matter* **2010**, *6*, 3395–3401.

28. Yao, X.; Peng, R.; Ding, J. Cell−Material Interactions Revealed *via* Material Techniques of Surface Patterning. *Adv. Mater.* **2013**, *25*, 5257–5286.

29. Kiessling, L. L.; Gestwicki, J. E.; Strong, L. E. Synthetic Multivalent Ligands as Probes of Signal Transduction. *Angew. Chem., Int. Ed.* **2006**, *45*, 2348–2368.

30. Doh, J.; Irvine, D. J. Photogenerated Polyelectrolyte Bilayers from an Aqueous-Processible Photoresist for Multicomponent Protein Patterning. *J. Am. Chem. Soc.* **2004**, *126*, 9170–9171.

31. Broyer, R. M.; Schopf, E.; Kolodziej, C. M.; Chen, Y.; Maynard, H. D. Dual Click Reactions to Micropattern Proteins. *Soft Matter* **2011**, *7*, 9972–9977.

32. Renault, J. P.; Bernard, A.; Juncker, D.; Michel, B.; Bosshard, H. R.; Delamarche, E. Fabricating Microarrays of Functional Proteins Using Affinity Contact Printing. *Angew. Chem., Int. Ed.* **2002**, *41*, 2320–2323.

33. Coyer, S. R.; García, A. J.; Delamarche, E. Facile Preparation of Complex Protein Architectures with Sub-100-nm Resolution on Surfaces. *Angew. Chem., Int. Ed.* **2007**, *46*, 6837–6840.

34. Christman, K. L.; Schopf, E.; Broyer, R. M.; Li, R. C.; Chen, Y.; Maynard, H. D. Positioning Multiple Proteins at the Nanoscale with Electron Beam Cross-Linked Functional Polymers. *J. Am. Chem. Soc.* **2009**, *131*, 521–527.

35. Lee, K.-B.; Lim, J.-H.; Mirkin, C. A. Protein Nanostructures Formed *via* Direct-Write Dip-Pen Nanolithography. *J. Am. Chem. Soc.* **2003**, *125*, 5588–5589.

36. Schvartzman, M.; Palma, M.; Sable, J.; Abramson, J.; Hu, X.; Sheetz, M. P.; Wind, S. J. Nanolithographic Control of the Spatial Organization of Cellular Adhesion Receptors at the Single-Molecule Level. *Nano Lett.* **2011**, *11*, 1306–1312.

37. Aydin, D.; Schwieder, M.; Louban, I.; Knoppe, S.; Ulmer, J.; Haas, T. L.; Walczak, H.; Spatz, J. P. Micro-Nanostructured Protein Arrays: A Tool for Geometrically Controlled Ligand Presentation. *Small* **2009**, *5*, 1014–1018.

38. Chai, J.; Huo, F.; Zheng, Z.; Giam, L. R.; Shim, W.; Mirkin, C. A. Scanning Probe Block Copolymer Lithography. *Proc. Natl. Acad. Sci. U.S.A.* **2010**, *107*, 20202–20206.

39. Kristensen, S. H.; Pedersen, G. A.; Ogaki, R.; Bochenkov, V.; Nejsum, L. N.; Sutherland, D. S. Complex Protein Nanopatterns over Large Areas *via* Colloidal Lithography. *Acta Biomater.* **2013**, *9*, 6158–6168.

40. Arnold, M.; Schwieder, M.; Blümmel, J.; Cavalcanti-Adam, E. A.; López-Garcia, M.; Kessler, H.; Geiger, B.; Spatz, J. P. Cell Interactions with Hierarchically Structured Nano-Patterned Adhesive Surfaces. *Soft Matter* **2008**, *5*, 72–77.

41. Lohmüller, T.; Aydin, D.; Schwieder, M.; Morhard, C.; Louban, I.; Pacholski, C.; Spatz, J. P. Nanopatterning by Block Copolymer Micelle Nanolithography and Bioinspired Applications. *Biointerphases* **2011**, *6*, MR1–MR12.

42. Zemła, J.; Lekka, M.; Raczkowska, J.; Bernasik, A.; Rysz, J.; Budkowski, A. Selective Protein Adsorption on Polymer Patterns Formed by Self-Organization and Soft Lithography. *Biomacromolecules* **2009**, *10*, 2101–2109.

43. Lau, K. H. A.; Bang, J.; Kim, D. H.; Knoll, W. Self-Assembly of Protein Nanoarrays on Block Copolymer Templates. *Adv. Funct. Mater.* **2008**, *18*, 3148–3157.

44. Kumar, N.; Parajuli, O.; Dorfman, A.; Kipp, D.; Hahm, J. Activity Study of Self-Assembled Proteins on Nanoscale Diblock Copolymer Templates. *Langmuir* **2007**, *23*, 7416–7422.

45. Shen, L.; Garland, A.; Wang, Y.; Li, Z.; Bielawski, C. W.; Guo, A.; Zhu, X.-Y. Two Dimensional Nanoarrays of Individual Protein Molecules. *Small* **2012**, *8*, 3169–3174.

46. Killops, K. L.; Gupta, N.; Dimitriou, M. D.; Lynd, N. A.; Jung, H.; Tran, H.; Bang, J.; Campos, L. M. Nanopatterning Biomolecules by Block Copolymer Self-Assembly. *ACS Macro Lett.* **2012**, *1*, 758–763.

47. Frith, J. E.; Mills, R. J.; Cooper-White, J. J. Lateral Spacing of Adhesion Peptides Influences Human Mesenchymal Stem Cell Behaviour. *J. Cell Sci.* **2012**, *125*, 317–327.

48. Hawker, C. J.; Russell, T. P. Block Copolymer Lithography: Merging "Bottom-Up" with "Top-Down" Processes. *MRS Bull.* **2005**, *30*, 952–966.

49. Kim, S. H.; Misner, M. J.; Xu, T.; Kimura, M.; Russell, T. P. Highly Oriented and Ordered Arrays from Block Copolymers *via* Solvent Evaporation. *Adv. Mater.* **2004**, *16*, 226–231.

50. Kim, T. H.; Hwang, J.; Acharya, H.; Park, C. Ordered Nanostructure of PS-B-PEO Copolymer by Solvent Annealing with Mixture of Benzene/Water Vapor and Its Micropattern Fabrication. *J. Nanosci. Nanotechnol.* **2010**, *10*, 6883–6887.

51. Zhu, L.; Tran, H.; Beyer, F. L.; Walck, S. D.; Li, X.; Ågren, H.; Killops, K. L.; Campos, L. M. Engineering Topochemical Polymerizations Using Block Copolymer Templates. *J. Am. Chem. Soc.* **2014**, *136*, 13381–13387.

52. Bates, F. S.; Fredrickson, G. H. Block Copolymers—Designer Soft Materials. *Phys. Today* **1999**, *52*, 32–38.

53. Son, J. G.; Chang, J.-B.; Berggren, K. K.; Ross, C. A. Assembly of Sub-10-Nm Block Copolymer Patterns with Mixed Morphology and Period Using Electron Irradiation and Solvent Annealing. *Nano Lett.* **2011**, *11*, 5079–5084.

54. Park, J. S.; Lee, S. H.; Han, T. H.; Kim, S. O. Hierarchically Ordered Polymer Films by Templated Organization of Aqueous Droplets. *Adv. Funct. Mater.* **2007**, *17*, 2315–2320.

55. Park, C.; Cheng, J. Y.; Fasolka, M. J.; Mayes, A. M.; Ross, C. A.; Thomas, E. L.; Rosa, C. D. Double Textured Cylindrical Block Copolymer Domains *via* Directional Solidification on a Topographically Patterned Substrate. *Appl. Phys. Lett.* **2001**, *79*, 848–850.

56. Onses, M. S.; Song, C.; Williamson, L.; Sutanto, E.; Ferreira, P. M.; Alleyne, A. G.; Nealey, P. F.; Ahn, H.; Rogers, J. A. Hierarchical Patterns of Three-Dimensional Block-Copolymer Films Formed by Electrohydrodynamic Jet Printing and Self-Assembly. *Nat. Nanotechnol.* **2013**, *8*, 667–675.

57. Olsen, B. D. Self-Assembly of Globular-Protein-Containing Block Copolymers. *Macromol. Chem. Phys.* **2013**, *214*, 1659–1668.

58. Reynhout, I. C.; Delaittre, G.; Kim, H.-C.; Nolte, R. J. M.; Cornelissen, J. J. L. M. Nanoscale Organization of Proteins *via* Block Copolymer Lithography and Non-Covalent Bioconjugation. *J. Mater. Chem. B* **2013**, *1*, 3026–3030.

59. Liu, D.; Wang, T.; Keddie, J. L. Protein Nanopatterning on Self-Organized Poly(styrene-b-isoprene) Thin Film Templates. *Langmuir* **2009**, *25*, 4526–4534.

60. Pierschbacher, M. D.; Ruoslahti, E. Cell Attachment Activity of Fibronectin Can Be Duplicated by Small Synthetic Fragments of the Molecule. *Nature* **1984**, *309*, 30–33.